24th September, 1992

PROPOSAL TO SEARCH FOR ANTIPROTON DECAY AT THE FERMILAB ANTIPROTON ACCUMULATOR

S. Geer†, J. Marriner, R. Ray, J. Streets
Fermi National Accelerator Laboratory, Batavia, Illinois 60510

C. Buchanan, B. Corbin, T. Muller, J. Quackenbush.
University of California, Los Angeles, California 90024-1547

R. Gustafson, L. Jones, G. Snow
University of Michigan, Ann Arbor, Michigan 48109

T. Armstrong, R.A. Lewis, G. Smith
Pennsylvania State University, University Park, Pennsylvania 16802

ABSTRACT

We propose to search for antiproton decay at the Fermilab antiproton accumulator. The experiment would search for decay modes in which there is an e^- or μ^- in the final state, and would be optimized to search for the decay mode $\bar{p} \rightarrow e^- + \pi^0$. We expect to achieve an experimental sensitivity to $\tau_{\bar{p}}$ x BR($\bar{p} \rightarrow e^- + \pi^0$) of up to O($10^8$ years), which is an improvement of 8 orders of magnitude over existing laboratory searches.

† Spokesperson

1. Introduction

The Fermilab antiproton source is a unique facility which affords the possibility of significantly improving the present laboratory limits on the antiproton lifetime, or of making the exciting discovery that the antiproton decays. We propose to search for antiproton decay at the Fermilab antiproton accumulator.

The positron and the antiproton are the only long lived antiparticles available in the laboratory for studying the stability of antimatter. The decay of the positron would require either a violation of charge conservation or the existence of a new very light positively charged particle. Thus, a search for antiproton decay seems to be the best way to test the stability of antimatter. Note that if the antiproton did decay with a lifetime much shorter than the age of the universe [$O(10^{10}$ years)] the predominance of matter over antimatter in the universe would be natural. Indeed the authors of Ref. 1 conclude that if we assume a conservative upper limit on the ratio of antiprotons to protons in the universe of 10^{-6} and attribute the smallness of this ratio to antiproton decay, then the antiproton lifetime is less than 2×10^8 years.

A short $\bar{p}$ lifetime ($\tau_{\bar{p}} < \tau_p$) would imply a violation of the CPT theorem. The CPT theorem is one of the most fundamental theorems of modern physics. We have no compelling reason to suspect a violation of CPT. However, CPT violation has been discussed in the literature[2], and in particular CPT violation has been discussed in connection with the generation of matter in the early universe[3]. It is important to subject the CPT theorem to continued experimental test. It should be noted that the way in which CPT violation would manifest itself in the laboratory is model dependent. Present limits on CPT violation based on searches for mass differences between particles and antiparticles do not necessarily exclude a short antiproton lifetime.

The best published antiproton lifetime limits from laboratory experiments are:

(i) $\tau_{\bar{p}} > 32$ hours, which was obtained[4] by observing the time evolution of 240 antiprotons in the ICE ring at CERN, where the beam lifetime was ~ 64 hours. An explicit search for $\bar{p} \rightarrow e^- + \pi^0$ was also made at the ICE ring[5] and yielded $\tau_{\bar{p}} \times BR(\bar{p} \rightarrow e^- + \pi^0) > 1700$ hours at 90% C.L. This search was made during a 10 day period in which the average number of antiprotons in the ring was 7200. The sensitivity of the experiment was limited by antiproton statistics. No explicit searches were made for other decay modes of the antiproton.

(ii) $\tau_{\bar{p}} > 1.4$ months, which was obtained[6] by storing antiprotons in the CERN Antiproton Accumulator for 11 days without adding or subtracting antiprotons, and measuring the storage lifetime.

(iii) $\tau_{\bar{p}} > 3.4$ months, which was obtained[7] by storing approximately 1000 antiprotons in an ion trap for about 2 months, and setting a limit on the containment lifetime in the trap. The sensitivity of the experiment is limited by the precision in knowing the number of antiprotons initially loaded into the trap.

Astrophysical considerations also suggest a limit on the antiproton lifetime. The measured[8] $\bar{p}/p$ ratio in cosmic rays of 5×10^{-4} is consistent with expectations for secondary production of antiprotons in the interstellar medium. This observation suggests that the antiproton lifetime is at least comparable to the cosmic ray storage time in the galaxy (yielding[9] $\tau_{\bar{p}} \geq 2 \times 10^6$ years). It should be noted that this result is not completely free of astrophysical assumptions, and at the present time is based on the observation of a single experiment.

The experiment we are proposing would search for explicit decay modes of the antiproton. Conservation of angular momentum requires that at least one of the daughter particles is a fermion (e, μ, or ν). The experiment will therefore search for decay modes in which there is an e^- or μ^- in the final state, and would be optimized to search for the decay mode $\bar{p} \rightarrow e^- + \pi^0$. Note that in many theories predicting proton decay, the equivalent decay mode $p \rightarrow e^+ + \pi^0$ has a large branching fraction (BR ~ 40% for SU(5) for example).

At the Fermilab antiproton source we anticipate typically $O(10^{12})$ antiprotons stored in the accumulator ring with a momentum of 8.9 GeV/c. Consider an experimental search for $\bar{p} \rightarrow e^- + \pi^0$, and suppose that the experiment runs for 2500 hours with 10^{12} antiprotons in the accumulator. Let the experimental geometrical acceptance be defined by a plane of trigger counters which are orthogonal to the beam axis, cover the full azimuthal angle, and extend from an inner radius with respect to the beam axis of 10 cm to an outer radius of 50 cm. The calculated fraction of $\bar{p} \rightarrow e^- + \pi^0$ decays in the accumulator ring for which all the final state particles pass within the geometrical acceptance is 7×10^{-3}. Thus, in the absence of background, taking into account the Lorentz factor of 9.5, one observed event in this hypothetical experiment would correspond to a lifetime $\tau_{\bar{p}} \times BR(\bar{p} \rightarrow e^- + \pi^0)$ of 2×10^8 years, which is an improvement 8 orders of magnitude over the present laboratory limit on this decay mode, two orders of magnitude over the indirect limit from cosmic ray

experiments, and reaches the upper limit on the antiproton lifetime (2×10^8 years) which is suggested if antiproton decay is responsible for the scarcity of antimatter in the universe.

2. The T861 Test

Potential backgrounds to the decay $\bar{p} \rightarrow e^- + \pi^0$ arise from cosmic rays, beam halo, beam-beam, beam-wall, and beam-gas interactions. A good understanding of background rates and characteristics is of crucial importance to the design of the experiment. To measure background rates and characteristics, we have installed a test setup (T861) in the AP50 region of the antiproton accumulator (Fig. 1). The test setup is shown in Fig. 2. It consists of a 5 meter long beampipe, the forward calorimeter from the E760 experiment, and additional trigger, vertex, and veto scintillation counters to better define the event topology. A more complete description of the test setup is given in Appendix 1. The T861 test was run parasitically at times when antiprotons were stored in the accumulator but stacking was not taking place. No dedicated beam time was required.

The trigger for the T861 test required a total energy deposited in the calorimeter E_{TOT} in excess of a threshold value. Trigger rates are summarized in Table 1. Setting the threshold to the low value of 20 MeV, the trigger rate was 5.9 KHz when antiproton stacking was not taking place, and there were 2.6×10^{11} antiprotons in the accumulator with a beam lifetime of 330 hours. This trigger rate is consistent with about 2% of the losses from the stored antiproton beam producing particles that enter the calorimeter. This can be approximately understood by noting that there is a 15.9 m straight section immediately upstream of the calorimeter, and that the total circumference of the ring is 474 m. The majority of the T861 test data were taken with a threshold $E_{TOT} > 1.5$ GeV, for which the trigger rate was reduced by about a factor of 17. In Fig. 3 the measured energy distribution using this trigger is compared with the predicted distribution for $\bar{p} \rightarrow e^- + \pi^0$. The GEANT Monte Carlo program was used to simulate the response of the T861 detector. The Monte Carlo simulation predicts that 1% of the antiproton decays, which are assumed to occur uniformly around the accumulator ring, result in one or more particles depositing energy in the calorimeter. The majority (70%) of the simulated antiproton decays which deposit some energy in the calorimeter result in a total energy deposition $E_{TOT} > 7$ GeV. In contrast to the Monte Carlo generated antiproton decays, the majority of the measured background events deposit much less than the total beam energy in the calorimeter. Requiring $E_{TOT} > 7$ GeV reduces the measured background event rate to O(0.1 Hz) whilst retaining 70% of the simulated decays that are within the geometrical acceptance of the calorimeter. Four typical events from the T861 test with $E_{TOT} > 7$ GeV are shown in Fig.

4. The topology of these events is different from the topology we would expect from the decay $\bar{p} \rightarrow e^- + \pi^0$. In the recorded events the calorimeter energy tends to be deposited in a single cluster, whilst in antiproton decays we would expect to see two or three clusters roughly balanced on either side of the beampipe. To quantify these differences we define (i) the cluster multiplicity N_{CLUST} as the number of calorimeter clusters found by a simple clustering algorithm[10], (ii) the energy centroids:

$$\bar{x} = \frac{\sum_i E_i x_i}{\sum_i E_i} \quad , \qquad \bar{y} = \frac{\sum_i E_i y_i}{\sum_i E_i} \quad ,$$

where the index i runs over the cells of the calorimeter. The measured distributions of $\bar{x}$, $\bar{y}$, and N_{CLUST} for events with $E_{TOT} > 7$ GeV are shown in Fig. 5 to be very different from the predicted distributions from antiproton decay. The requirements $E_{TOT} > 7$ GeV, $\bar{x} < 4$ cm, $\bar{y} < 4$ cm, and $2 \leq N_{CLUST} \leq 3$, retain 60% of the simulated decays that are within the geometrical acceptance of the calorimeter, whilst reducing the event rate to 4 x 10^{-3} Hz. Examples of events that survive these cuts are shown in Fig. 6. Given the limitations of the T861 test setup we are not able to determine the origin of these events: they could arise from beam-gas, beam-wall, or beam-halo interactions, or even from genuine antiproton decays. The T861 test results enable us to conclude that:

i) The simple calorimeter trigger (E_{TOT} > a few GeV) we have employed in the T861 test reduces the trigger rate to a manageable level.

ii) Simple cuts based on calorimeter information alone eliminate the majority of background events. Taking the detector efficiency into account, but not accounting for systematic uncertainties, we deduce that the sensitivity of the T861 test using calorimeter information alone corresponds to $\tau_{\bar{p}}$ x BR($\bar{p} \rightarrow e^- + \pi^0$) of the order of 1000 years.

iii) To achieve a sensitivity to $\tau_{\bar{p}}$ x BR($\bar{p} \rightarrow e^- + \pi^0$) of up to O($10^8$ years) we need to improve the background rejection by a factor of ~ 10^5.

iv) To determine the origin of the surviving events from the T861 test analysis we need to improve some aspects of the experimental setup. In particular we need to improve the vacuum in the decay volume, reduce the amount of material traversed by particles exiting the decay volume before entering the detector, and improve the electron identification.

v) Our experience with the T861 test has led us to believe that the next step in the experiment can also be done parasitically with no dedicated beam time requested, unless we see indications of a signal.

3. Proposal for the Antiproton Decay Search Experiment

We propose to upgrade the T861 test setup in two stages. Stage I would be at the beginning of run Ib, and would be expected to be sensitive to $\tau_{\bar{p}}$ x BR($\bar{p} \rightarrow e^- + \pi^0$) of up to O($10^5$ years) or better. The stage I data would be taken parasitically at the antiproton accumulator during times when stacking was not taking place, would enable a search for decay modes of the antiproton in which there was an electron in the final state, and would enable a study of remaining backgrounds, which would assist in the design of the stage II experiment. The stage II experiment would take place during run II. Stage II would have upgraded calorimetry, tracking, and lepton identification, as necessary in order to be sensitive to decays with $\tau_{\bar{p}}$ x BR($\bar{p} \rightarrow e^- + \pi^0$) < O($10^8$ years), and make possible the search for decay modes in which there is a muon in the final state.

A schematic layout of the proposed setup for the stage I experiment is shown in Fig. 7. The experiment is optimized to observe the decay mode $\bar{p} \rightarrow e^- + \pi^0$ in the presence of a large background of beam-gas interactions in the vicinity of the apparatus, and of spray from interactions further upstream. To illustrate the expected sensitivity of the stage I experiment, assume that the antiproton lifetime x branching ratio is 10^5 years, and that beam conditions are similar to those for the T861 test (2.6 x 10^{11} antiprotons in the accumulator). After 100 hours of data taking we would observe 19 decays, where we have taken into account the fraction of decays contained in the detector (0.01), calorimeter cut efficiencies (0.6), and the Lorentz factor of 9.5. If we improve on the background rejection of the T861 setup by a factor of 10^3, then the expected background passing our cuts after 100 hours of data taking would be 1.4 events. Thus we would observe a very significant signal.

The experiment is designed to achieve a high background suppression in order to have sensitivity to small signals that could be due to antiproton decay. In the stage I experiment we aim to improve the background rejection already achieved in the T861 test by a factor of 10^3 . The major features of the stage I experiment that allow it to achieve this are:

(i) A large high vacuum fiducial volume to reduce beam gas interactions.

(ii) Upstream veto counters to reduce spray from upstream interactions.

(iii) Full kinematic identification of the final state, including:

a. Full reconstruction of the electron momentum via tracking and calorimetry. When combined with the knowledge of the beam momentum, this measurement alone provides one kinematic constraint on the final state.

b. Full reconstruction of the π^0. This provides three additional kinematic constraints on the final state.

(iv) Identification of the prompt electron.

The major elements of the experiment are discussed in turn below:

3.1 Vacuum Chamber

The vacuum system for the proposed experiment needs to meet the following two criteria:

a) The residual gas pressure inside the decay volume should be as low as possible. This will reduce the rate of antiproton beam-gas interactions that fake an antiproton decay signal. Clearly, there is no particular vacuum that is "good enough" - the lower the vacuum the better.

b) The material (radiation lengths) between the decay point and the detector should be minimized. Minimizing the number of radiation lengths, and hence the number of conversions in front of the detector, allows us to exploit the prompt electron signature from the $\bar{p} \rightarrow e^- + \pi^0$ decay. A reasonable criterion is to limit the material to approximately 1% of a radiation length so that conversions in the window are comparable to the rate of Dalitz decays of the π^0 ($\pi^0 \rightarrow \gamma + e^+ + e^-$).

3.1.1 Conceptual Design of the Vacuum Tank

A variety of technologies are available to achieve ultra-high-vacuum. The most effective technologies use cryogenic techniques, but we have ruled these out because of the high costs that would be involved. A relatively inexpensive technology that can be used for systems with moderate gas loads is based on titanium sublimation pumps. We believe that use of this technology will allow us to improve the T861 vacuum by more than one order of magnitude, and achieve a residual vacuum pressure of less than 10^{-11} torr. The vacuum

vessel will undergo a high temperature vacuum degas cycle and will be equipped with heaters and blankets for an in–situ bakeout at 350 ^{o}C.

To minimize the number of radiation lengths traversed by the electron we have chosen a conceptual design with a thin downstream window (Fig. 8). Based on the proposed FNAL engineering standard for vacuum windows, the window thickness would lie in the range of 0.6 mm to 1.3 mm, depending on the material used. Possible choices of material for the window include beryllium (0.3% radiation length per mm), high strength aluminum (1% radiation length per mm), titanium (3% radiation length per mm), and stainless steel (6% radiation length per mm). The design and fabrication of the window will require a significant mechanical engineering effort.

3.1.2 Accelerator Physics Issues

There are accelerator physics issues associated with the use of the proposed vacuum tank in the accumulator ring. Ions produced by the antiprotons will naturally accumulate in the tank. These ions can drive beam instabilities. However, the ions can be substantially reduced with clearing electrodes similar to those used elsewhere in the accumulator. The clearing electrodes will also provide a convenient pressure gauge (typical ion gauges have poor signal to noise ratios at 10^{-11} torr). A large vacuum tank can in principle present a significant impedance to the beam. Although we have not made any calculations, we believe that a combination of factors will ameliorate the potential problems, namely:

a) The tank is likely to be several wavelengths long at even the lowest order modes.

b) The Q of the tank will be relatively low (perhaps 1000). If necessary the tank can be considerably de-Q-ed by the addition of external loads.

3.2 Movable Target

A target that can be moved remotely in or out of the beam halo immediately upstream of the decay volume will provide a source of localized interactions that can be used (i) to understand and align the tracking elements of the detector, and (ii) to provide a vertex constraint for reconstruction of $\bar{p}$ - nucleon interactions in the detector, which will aid in understanding event reconstruction and help provide an in-situ calibration of the calorimeter. The calibration of the calorimeter was confirmed in E760 running by reconstructing a π^0 peak (Fig. 9) in the two-photon mass spectrum. The reconstructed

mass was 130 ± 1 MeV/c^2 with an rms width of 18 ± 1 MeV/c^2. This calibration was possible because the E760 gas-jet target provided a localized source of interactions.

3.3 Calorimeter

We propose to continue to use the forward calorimeter of the E760 experiment. A schematic of the calorimeter is shown in Fig. 2. The calorimeter consists of an array of 10 x 10 cm^2 lead scintillator blocks that are 17.7 radiation lengths deep. The details of the calorimeter construction and performance have been published[13]. The measured energy resolution of the calorimeter is:

$$\frac{\sigma}{E} = \left[\left(\frac{0.08}{\sqrt{E[GeV]}} \right)^2 + (0.068)^2 \right]^{1/2}.$$

For electrons in the range of interest (1-8 GeV) the energy resolution will range from 11% to 7%. The calorimeter does not have longitudinal segmentation and has fairly coarse transverse segmentation. Hadronic showers are not normally fully contained in the calorimeter. However, a $\bar{p} \rightarrow e^- + \pi^0$ decay in which the electron and photon showers are contained transversely in the calorimeter will result in the observation of the full beam energy.

3.4 Tracking

A position detector constructed from 2mm diameter blue scintillating fibers and Hamamatsu R4135A multianode PMTs has recently been constructed. Testbeam results[11] are encouraging, and we therefore propose to use this technology for measuring the electron candidate tracks emerging from the vacuum chamber. We intend to use four 90 x 90 cm^2 planes of fibers arranged as shown in Figs. 7 and 10. The upstream horizontal and vertical planes (H1 and V1) will be separated from the downstream planes (H2 and V2) by about 1 meter. Each plane will consist of 800 fibers 90 cm long and 200 fibers 40 cm long. To reduce the number of channels read out, the fibers will be grouped in pairs on the input of the PMTs. Thus there will be 1000 fibers read into 500 input channels per plane. Each plane will be readout using 4 PMTs, which are designed to read up to 224 input channels, with the readout multiplexed into 36 output channels. We would use 125 input channels per tube multiplexed into 32 output channels. Thus for four scintillating fiber planes we require 16 PMTs and 512 output channels.

The tracking will enable the direction of outgoing electron candidates to be determined with an angular resolution of 2 mrad. The lack of redundancy and the lack of stereo information is not expected to be a limitation because the final state of interest has a single charged track. We use the tracking in three ways. First, the measured polar decay angle, together with the measured electron energy in the calorimeter, uniquely determine the antiproton decay kinematics. Second, the electron can be extrapolated to the beam and the vertex position in z (along the beam axis) can be determined crudely (0.5 m). This will enable rejection of interactions outside of the fiducial volume of the experiment. Finally, the vertex position, together with the calorimeter cluster information, can be used to determine the π^o momentum.

3.5 Upstream Veto Counters

These counters are not technically challenging and we do not expect any counter to have a counting rate in excess of 10 kHz. However, the counters will be designed to operate up to 1 MHz to avoid possible problems with pile-up. These counters could be similar or identical in design to the dE/dx counters discussed below.

3.6 Decay Volume Veto Counters

Because of the kinematics of the decay $\bar{p} \rightarrow e^- + \pi^o$, in the laboratory frame both the electron and the π^o tend to be emitted at small angles with respect to the beam direction. We can take advantage of this by placing wide angle veto counters around the outside of the vacuum tank. Typical interactions with the residual gas will produce wide angle particles from the fragmentation of the target nucleus. The wide angle veto counters can be used to reject such events. The effectiveness of this veto system, however, will be limited by two facts. First, the area to be covered is large - about 15 m^2, and we may not be able to economically cover the entire area. Second, we expect the tank wall to be about 0.5" thick. Protons with momentum less than 300 MeV/c and pions less than 100 MeV/c will not penetrate the wall. Higher momentum particles can be detected depending on the angle of incidence and whether they interact in the wall or not. However, we expect that even partial coverage will be useful in giving us a handle on beam gas backgrounds.

In the stage I experiment we propose to install veto counters that will cover about 30% of the decay volume. This will provide us with a test to evaluate the importance of covering the entire decay volume for the stage II experiment. To minimize costs we would use existing counters recovered from the completed E715 fixed target experiment.

3.7 Downstream Veto Counters

To veto interactions which result in particles that enter the calorimeter after exiting the beam pipe downstream of the decay volume, we propose to surround the beam pipe in this region with veto scintillation counters (Fig. 7). These counters are not technically challenging, and cover a relatively modest surface area.

3.8 dE/dx Counters

A potential background comes from $\bar{p}p$ annihilation into a small number of π^o's. Photons that convert in the window or Dalitz pairs will look like electrons in the tracking planes and in the calorimeter. To suppress these backgrounds we intend to use two planes of 1/2" thick dE/dx scintillation counters (dEdx1 and dEdx2) as shown in Figs. 7 and 11. Note that over most of its acceptance, each plane provides two dE/dx measurements. These counters will be designed to keep the pulse height uniform over their entire area to the level of ±5%. As an example of how well we expect these counters to perform, Fig. 12 shows the pulse height spectrum obtained in the E715 hyperon experiment which used four planes of 1/4" thick scintillation counters of similar lateral dimensions and design to the ones we are proposing. Single, double, and triple minimum ionizing peaks are cleanly separated.

3.9 Pre-radiator

To compensate for the fact that the calorimeter has no longitudinal segmentation we plan to install a lead "pre-radiator" upstream of the calorimeter. The pre-radiator will be about 0.5" thick (2.3 radiation lengths and 0.12 interaction lengths). Scintillators behind the pre-radiator will normally measure a pulse-height greater than minimum ionizing for electrons, but only minimum ionizing for pions. These scintillators (dEdx3 as shown in Fig. 7) will be of the same design as the dE/dx counters described above. We plan to use the pre-radiator in the off-line analysis to distinguish between electrons and pions that are fully contained in the calorimeter.

3.10 Trigger

A number of the features expected for antiproton decay could provide possible triggers for the experiment. In particular, signals from the veto counters, summed signals from the calorimeter towers, pulse height from the dE/dx counters, and particle trajectories in the scintillating fiber tracking would enable us to use:

(i) Absence of an upstream or downstream veto counter hit.

(ii) Minimum total energy deposition in the calorimeter.

(iii) Transverse momentum balance in the calorimeter.

(iv) Absence of a decay volume veto counter hit.

(v) Pulse height in the dE/dx counters.

(vi) Hits in the scintillating fibers.

(vii) Position and angle correlations in the tracking.

(viii) Correlations between calorimetry energy and decay angle.

Currently, we plan to use requirements (i) - (iii) in the trigger. The first requirement can be implemented very simply. The second can be accomplished with existing circuitry (used in the T861 test run). The third requirement can be achieved (crudely) by recabling the existing circuitry. The calorimeter block will divided into 4 quadrants as shown for example in Fig. 13. The pulse height will be summed for each quadrant separately. The trigger will require 1.5 GeV or more in 2 or more quadrants of the detector. Thus, we will require a total 3.0 GeV threshold and a topology consistent with transverse momentum balance.

The experiment clearly has a wealth of information that could be added to the trigger if required. However, we expect that our very simple trigger will be entirely adequate.

3.11 Data Acquisition

We expect the trigger to reduce the background rate to 30 Hz or less. A one hour run would log 100,000 events. The existing VAXONLINE data acquisition, which is described in the appendix, would be adequate for our needs. CAMAC and FASTBUS modules will be read via Jorway and LeCroy interfaces into a VAX, and events written to 8mm Exabyte tapes.

Table 6 lists the items we will need to borrow from PREP for the data acquisition. We would plan to use as much of the existing front end electronics from the E760 experiment as possible, supplemented with additional crates and a VAX and associated peripherals in order to be able to run independently of P835 tests.

3.12 Offline Requirements

Assuming a trigger rate of 30 Hz, and a total live time of 100 hours, in the stage I experiment we would expect to write 11 million events to 8mm tape. The event size will be about 1000 words, and hence the full dataset size is expected to be of order 44 Gbytes, which will fit onto 22 single density 8mm tapes. A pre-filter on calorimeter information alone should provide a rejection factor of at least 10^3, reducing the dataset size to < 40 Mbytes, which we would wish to put on non-backed-up disk for easy access.

The CPU requirements for the experiment will be dominated by the Monte Carlo studies required to understand the data sample and design the stage II experiment. Assuming that 50% of the Monte Carlo samples will be generated at the outside institutions, and 50% at Fermilab, we estimate that to simulate 10^6 background interactions using the GEANT program we would require of order 3000 VAX 780 hours at Fermilab.

3.13 Beam-Gas Background Monte Carlo

The scintillating fiber planes and upstream veto counters should enable us to reduce the beam-halo and beam-wall interactions to a negligible level. The dominant backgrounds for the stage I experiment are expected to arise from beam-gas interactions. To understand the beam-gas interaction backgrounds, a good understanding of $\bar{p}p$ and $\bar{p}n$ interactions at 8.9 GeV/c is needed. Several measurements of exclusive, semi-inclusive, and topological cross-sections and event kinematics have been reported in the literature for $\bar{p}p$[12,13,14] and $\bar{p}n$[15] interactions in the vicinity of 8.9 GeV/c. Measured topological cross-sections are summarized in Table 2, and measured cross sections for exclusive final states are summarized in Table 3. The measurements enable a realistic simulation to be made of beam-gas background interactions at the antiproton accumulator. We have developed a $\bar{p}p$ and $\bar{p}n$ beam-gas Monte Carlo generator in which each exclusive final state is explicitly generated for all annihilation processes with less than twelve final state particles, and all non-annihilation processes with less than ten final state particles. The measured cross-sections have been input into the $\bar{p}p$ event generator for all the processes listed in Tables 3a and 3b. This accounts for 73% of the total $\bar{p}p$ cross-section at 8.9 GeV/c. Reasonable guesses have been made for the cross-sections of the unmeasured processes, tuned so that the generator reproduces the measured semi-inclusive and topological cross-sections (Table 2). Coulomb scattering has also been implemented, taking into account the measured residual gas composition in the accumulator. The measured kinematics for elastic scattering and for three-body non-annihilation final states have been explicitly implemented in the

Monte Carlo event generator. All other processes have been generated with a longitudinal phase space generator, where the mean transverse particle momenta were adjusted to reproduce, as a function of the number of final state particles, the measured transverse momenta in annihilation and non-annihilation events (Table 4).

4. Stage II Experiment

We plan to upgrade the stage I experiment to achieve the ultimate sensitivity of $O(10^8)$ years, and to extend the search to include decay channels in which there is a final state muon. The design of the stage II experiment will be aided by the lessons learnt in the stage I experiment. Given the parasitic nature of the experiment, stage II will need to be installed for the entire run II period, and possibly beyond, in order to accumulate a total of O(1000 hours) of data taking. We therefore anticipate the need to construct a radiation hard calorimeter for this final phase of the experiment. We also anticipate the need for improved tracking and the addition of muon chambers behind the calorimeter in order to search for final state muons. Other upgrades for improved electron identification may be required.

5. Cost and Schedule

A cost estimate for the stage I experimental setup is given in Table 5. A PREP list for the data acquisition system is given in Table 6. The milestones we would like to achieve are summarized as follows:

Feb. 1993	Completed design of vacuum chamber and scintillating fiber tracking.
May 1993	Complete construction of vacuum chamber, scintillating fiber tracking planes, and scintillation counters ready for installation.
Run 1b Startup	Commission stage I detector.
Run 1b; month 1	Data taking
Run 1b; month 2	De-install calorimeter in a convenient access.
End of Run 1b	Proposal for stage II experiment.

Appendix 1: The T861 Test Setup

The T861 test was largely based on pre-existing equipment, and was not optimized to search for antiproton decay. A description of the test setup is given below:

i) Beampipe

The T861 test used a 5 meter long stainless steel vacuum pipe with a diameter of 3 inches, and a wall thickness of 0.7 mm.

ii) Vacuum

The vacuum inside the beampipe for the T861 test was not optimal. The bakeout temperature of the pipe varied along its length from about 130°C to about 250°C. Ion and sublimation pumps were installed at either end of the pipe. The measured vacuums at the pipe ends were 3×10^{-10} Torr at the upstream end and 8×10^{-11} Torr at the downstream end. An analysis of the residual gas composition was made using a mass spectrometer. The results showed the presence of hydrogen (220×10^{-12} Torr), CH_4 (7×10^{-12} Torr), H_2O (38×10^{-12} Torr), CO (24×10^{-12} Torr), and CO_2 (10×10^{-12} Torr). With this gas composition we would expect that ~64% of the beam-gas interactions come from $\bar{p}p$ interactions and 36% come from $\bar{p}n$ interactions.

iii) Calorimetry

The T861 test used the forward electromagnetic sampling calorimeter of the E760 experiment. Some details of the calorimeter are shown in Fig. 2 and a full description is given in ref. 16. The calorimeter consists of 144 rectangular modules arranged in a 13 x 13 array with six modules at each of the four corners absent. Each module consists of 148 alternate layers of lead and acrylic scintillator plates with transverse dimensions of 10 x 10 cm^2. The lead plates are 1 mm thick. The first 32 scintillator plates are 0.64 cm thick, and the remaining 42 plates are alternately 0.64 cm and 0.32 cm thick, resulting in an active length of the module of 48.4 cm (17.7 radiation lengths). The calorimeter was designed for the detection of low energy (< 1 GeV) photons. However, the calorimeter linearity has been checked using 1 GeV and 3 GeV electron beams at BNL. The non-linearities do not

exceed a few percent in this energy range. The resolution of the calorimeter for E760 running is given by :

$$\frac{\sigma}{E} = \left[\left(\frac{0.08}{\sqrt{E}[GeV]} \right)^2 + (0.068)^2 \right]^{1/2},$$

where the calibration was obtained in part by using insitu processes. In the absence of this extra calibration check, the calorimeter calibration for the T861 test is given by :

$$\frac{\sigma}{E} = \frac{0.2}{\sqrt{E}[GeV]} .$$

iv) Event Topology

Vertex, trigger, and veto scintillation counters were installed for the T861 test to help define the event topology. The vertex position counters consist of two 100 x 15 cm^2 counters, one placed on the left side and one on the right side of the beampipe (Fig. 2), located such that their downstream ends were 208 cm upstream of the calorimeter face. The vertex counters were read out at both ends to determine the exit position of traversing particles leaving the beampipe. At the upstream end of the vertex counters, four 100 x 10 cm^2 veto counters were arranged to form a veto box around the beampipe to flag the presence of additional particles exiting at large angle from the vertex region. In front of the calorimeter face four 30 x 30 cm^2 trigger counters were installed, one pair on the left side and one pair on the right side of the beampipe. The downstream members of each pair were 10 cm upstream of the calorimeter face, and the upstream members were 20 cm upstream of the calorimeter face. This arrangement of vertex, trigger, and veto counters enabled the selection of events which originate from a vertex approximately 350 ± 50 cm upstream of the calorimeter, and for which two outgoing particles, which are coplanar with the beam axis, enter the calorimeter, and for which no additional charged particles leave the vertex at large angle and traverse the veto counters.

v) Trigger and Data Acquisition

The T861 test used the existing trigger electronics and data acquisition system of the E760 experiment. Signals from the trigger and veto counters, and six summed signals from the calorimeter cells, were used to trigger the readout. Calorimeter and

counter signals were digitized, latched, and counted with E760 cables, CAMAC front end modules, clocks and scalars.

Events were taken using the VAXONLINE[17] data acquisition software, which uses a CAMAC Jorway interface connected to a microVAX II front end computer. By changing the standard event builder, we were able to increase the maximum trigger rate from 60 Hz to 500 Hz. The event sizes were approximately 100 bytes. We obtained event rates of 150 Hz when writing to 8mm Exabyte tapes.

Online monitoring was performed with E760 histogram viewer and event display programs modified for the different event source and T861 event format.

References

[1] D. Cline, P. McIntyre, and C. Rubbia, Phys. Lett. 66B(1977)429.

[2] Ch. Ragiadakos and Ch. Zenses, Phys. Lett. 76B(1978)61.
B. Kenny and R. Sachs, Phys. Rev. D8(1973)1605.

[3] E. Kolb and M. Turner, "The Early Universe", Frontiers in Physics Lecture Note Series, Addison-Wesley Publishing Company, Inc.

[4] M. Bregman et al., Phys. Lett. 78B (1978) 174.

[5] M. Bell et al., Phys. Lett. 86B (1979) 215.

[6] B. Autin et al; reported at the European Particle Accelerator Conference, 1990.

[7] G. Gabrielse et al; Phys. Rev. Lett. 65 (1990) 1317.

[8] R.L. Golden et al., Phys. Rev. Lett. 43 (1979) 1196.

[9] The Particle Data Book quotes $\tau_{\bar{p}} \geq 10^7$ years. However, this does not take into account the relativistic γ-factor of the antiprotons detected in the cosmic ray experiment. A more careful analysis by D. Kennedy (private communication) yields $\tau_{\bar{p}} \geq 2 \times 10^6$ years.

[10] The calorimeter clustering algorithm we used identifies the highest energy available cell in the calorimeter as a seed cell, and forms a cluster by associating all available cells in a 3 x 3 grid around the seed cell. An available cell is one with a deposited energy in excess of 50 MeV which has not been previously associated with a cluster. The clustering algorithm is repeated until there are no available cells remaining.

[11] J. Hauser et al; preprint UCLA-HEP-92-003 (1992), Submitted to Nucl. Instr. & Methods.

[12] P.S.Gregory et al., Nucl. Phys. B119(1977)60.

[13] A.J.Simmons et al., Nucl. Phys. B172(1980)285.

[14] D.R.Ward et al., Nucl. Phys. B172(1980)302.

[15] H.Braun et al., Proc. 5th European Symp. on Nucleon Antinucleon int., Bressanone, 1980.

[16] M.A.Hasan et al., Nucl. Instr. and Meth. A295 (1990)73.

[17] V. White et al., IEEE Transactions on Nuclear Science, Vol.NS-34, No.4, August 1987.

Table 1: Measured trigger rates from the T861 test; measurements were made with 2.6×10^{11} antiprotons in the accumulator and a beam lifetime of 330 hours.

	Rate (Hz)
Calorimeter $E_{TOT} > 20$ MeV	5900
Calorimeter $E_{TOT} > 1.5$ GeV	350
Trigger Counter Singles Rate	680
Vertex Position Counter Singles Rate	700
Veto Box Rate	2700

Table 2a: Measured topological cross sections for $\bar{p}p$ interactions at 8.8 GeV/c (C.N.Booth et al; Phys. Rev. D27(1983)2018) and 9.1 GeV/c (P.S.Gregory et al; Nucl. Phys. B119(1977)60).

Prong Number	**Cross section (mb)**	
	8.8 GeV/c	**9.1 GeV/c**
0	2.35 ± 0.06	2.58 ± 0.08
2 (elastic)	12.33 ± 0.40	11.75 ± 0.23
2 (inelastic)	14.63 ± 0.30	15.57 ± 0.54
4	16.79 ± 0.21	17.37 ± 0.18
6	7.68 ± 0.12	7.97 ± 0.12
8	1.86 ± 0.05	2.01 ± 0.06
10	0.23 ± 0.02	0.23 ± 0.02
12	0.017 ± 0.005	0.03 ± 0.01
TOTAL	55.90 ± 1.5	57.51 ± 0.73

Table 2b: Measured topological cross sections for $\bar{p}n$ interactions at 9.2 GeV/c (H. Braun et al; Proc. 5th European Symp. Nucleon Antinucleon Interactions, Bressanone, June 1980).

Prong Number	**Cross section (mb)**
3	13.3 ± 0.7
5	8.9 ± 0.6
7	3.7 ± 0.3
9	0.82 ± 0.10
11	0.08 ± 0.03
13	0.008 ± 0.008

Table 3a: Measured cross sections for $\bar{p}p$ annihilations at 8.8 GeV/c (D.R.Ward et al; Nucl. Phys. B172(1980)302) and 9.1 GeV/c (P.S.Gregory et al; Nucl. Phys. B119(1977)60).

Final State	Cross section (mb)	
	8.8 GeV/c	9.1 GeV/c
$\pi^+\pi^-$	0.004 ± 0.002	
$\pi^+\pi^-\pi^0$	0.03 ± 0.01	0.02 ± 0.01
$2\pi^+2\pi^-$	0.046 ± 0.008	0.048 ± 0.006
$2\pi^+2\pi^-\pi^0$	0.50 ± 0.04	0.53 ± 0.02
$3\pi^+3\pi^-$	0.140 ± 0.014	0.16 ± 0.01
$3\pi^+3\pi^-\pi^0$	0.958 ± 0.05	0.94 ± 0.03
$4\pi^+4\pi^-$	0.08 ± 0.01	0.09 ± 0.01
$4\pi^+4\pi^-\pi^0$	0.28 ± 0.03	0.48 ± 0.03
$5\pi^+5\pi^-$	0.020 ± 0.006	
$5\pi^+5\pi^-\pi^0$	0.041 ± 0.007	

Table 3b: Measured cross sections for $\bar{p}n$ annihilations at 9.2 GeV/c (H. Braun et al; Proc. 5th European Symp. Nucleon Antinucleon Interactions, Bressanone, June 1980).

Final State	Cross section (mb)
$\pi^+\pi^-\pi^-$	≤ 0.0003
$\pi^+2\pi^-\pi^0$	0.11 ± 0.02
$2\pi^+3\pi^-$	0.08 ± 0.01
$2\pi^+3\pi^-\pi^0$	0.66 ± 0.04
$3\pi^+4\pi^-$	0.11 ± 0.02
$3\pi^+4\pi^-\pi^0$	0.59 ± 0.05
$4\pi^+5\pi^-$	0.052 ± 0.005
$4\pi^+5\pi^-\pi^0$	0.17 ± 0.02

Table 3c: Measured cross sections for $\bar{p}p$ non-annihilation events at 8.8 GeV/c (D.R.Ward et al; Nucl. Phys. B172(1980)302) and 9.1 GeV/c (P.S.Gregory et al; Nucl. Phys. B119(1977)60).

Final State	**Cross section (mb)**	
	8.8 GeV/c	**9.1 GeV/c**
$\bar{p}p$	11.5 ± 0.4	11.75 ± 0.23
$\bar{p}p\pi^0$	1.27 ± 0.08	1.31 ± 0.03
$\bar{p}n\pi^+$	1.35 ± 0.09	1.40 ± 0.03
$\bar{n}p\pi^-$	1.36 ± 0.09	1.40 ± 0.04
$\bar{p}p\pi^+\pi^-$	2.40 ± 0.06	2.60 ± 0.05
$\bar{p}p\pi^+\pi^-\pi^0$	2.04 ± 0.06	2.04 ± 0.04
$\bar{p}n\pi^+\pi^+\pi^-$	1.02 ± 0.04	0.98 ± 0.03
$\bar{n}p\pi^-\pi^-\pi^+$	1.02 ± 0.04	0.98 ± 0.03
$\bar{p}p2\pi^+2\pi^-$	0.45 ± 0.03	0.48 ± 0.02
$\bar{p}p2\pi^+2\pi^-\pi^0$	0.50 ± 0.03	0.48 ± 0.02
$\bar{p}n3\pi^+2\pi^-$	0.32 ± 0.02	0.19 ± 0.01
$\bar{n}p3\pi^-2\pi^+$	0.32 ± 0.02	0.19 ± 0.01
$\bar{p}p3\pi^+3\pi^-$	0.020 ± 0.006	0.02 ± 0.005
$\bar{p}p3\pi^+3\pi^-\pi^0$	0.03 ± 0.01	0.02 ± 0.005
$\bar{p}n4\pi^+3\pi^-$	0.02 ± 0.01	0.01 ± 0.004
$\bar{n}p4\pi^-3\pi^+$	0.02 ± 0.01	0.01 ± 0.004
$\bar{p}p4\pi^+4\pi^-$	0.001 ± 0.001	

Table 4a: Measured mean transverse momenta in $\bar{p}p$ annihilations at 8.8 GeV/c (D.R.Ward et al; Nucl. Phys. B172(1980)302).

Final State	**Mean p_T (GeV/c)**
$2\pi^+2\pi^-$	0.53 ± 0.02
$2\pi^+2\pi^-\pi^0$	0.477 ± 0.006
$3\pi^+3\pi^-$	0.43 ± 0.01
$3\pi^+3\pi^-\pi^0$	0.389 ± 0.004
$4\pi^+4\pi^-$	0.36 ± 0.01
$4\pi^+4\pi^-\pi^0$	0.323 ± 0.006

Table 4b: Measured mean transverse momenta in $\bar{p}p$ non-annihilation events at 8.8 GeV/c (D.R.Ward et al; Nucl. Phys. B172(1980)302).

Final State	Mean p_T (GeV/c)
$\bar{p}p\pi^+\pi^-$	0.322 ± 0.003
$\bar{p}p\pi^+\pi^-\pi^0$	0.369 ± 0.003
$\bar{p}p2\pi^+2\pi^-$	0.331 ± 0.006
$\bar{p}p2\pi^+2\pi^-\pi^0$	0.308 ± 0.004

Table 5: Cost Estimate (K$).

Item	New	Existing
Vacuum Tank		
Tube + Bellows (material)	6	
Tube (fabrication)	13	
Upstream + Downstream Flanges	6	
Downstream Window	5	
Sublimation Pumps and Clearing Electrodes	6	
Vacuum Degas	3	
Bakeout Heaters/blankets	5	
Sub-Totals	**44**	**0**
Movable Target		
Bellows, Body & Mechanism	3	
Stand and Motors	2	
Fabrication	5	
Sub-Totals	**10**	**0**
Scintillating Fiber Tracking		
Fibers (4000)	18	
Multi-anode Photomultiplier Tubes (16)		48
Supports	2	
Sub-Totals	**20**	**48**
Calorimeter		
Sub-Totals		**100**
Upstream Veto Counters		
Scintillator + light guides (4 counters: 100 cm x 50 cm x 1/4")	6	
Photomultiplier Tubes + Bases (4)	6	
Supports	2	
Sub-Totals	**14**	**0**
Decay Volume Veto Counters		
Scintillator + light guides (4 counters: 111.8 cm x 66 cm x 1/4")		6
Photomultiplier Tubes + Bases (4)		6
Supports	4	
Sub-Totals	**4**	**12**
Downstream Veto Counters		
Scintillator + light guides (4 counters: 150 cm x 10 cm x 1/2")	5	
Photomultiplier Tubes + Bases (4)	6	
Supports	1	
Sub-Totals	**12**	**0**
dE/dx Counters (dEdx1 and dEdx2)		
Scintillator + light guides (8 counters: 100 cm x 50 cm x 1/2")	13	
Photomultiplier Tubes + Bases (16)	24	
Supports	4	
Sub-Totals	**41**	**0**
Pre-radiator (dEdx3)		
Scintillator + light guides (4 counters: 100 cm x 50 cmx 1/2")	7	
Photomultiplier Tubes + Bases (8)	12	
Supports	2	
Sub-Totals	**19**	**0**
Cables		
Position Detector	15	
Sub-Totals	**15**	
TOTAL	**179**	**160**
Contingency (20%)	**36**	
TOTAL with Contingency	**215**	

Table 6: PREP list for the Data Acquisition and Trigger Electronics.

Quantity	Description
VAX plus PERIPHERALS	
1	VAX VMS 3200 with monitor plus operating software, plus Ethernet connection to Lab.
2	Terminals (VT1lent) if 3200 has no monitor.
1	Graphics terminal if 3200 has no monitor.
1	Laser printer.
1	QBUS SCSI controller.
1	Wren VII disk.
1	Exabyte tape unit.
CAMAC	
1	Jorway 411 CAMAC interface
1	CAMAC branch highway cable
1	CAMAC crate plus power supply
1	A-2 CAMAC crate controller
1	CAMAC branch highway terminator
1	LAM latch module
1	Scaler LRS 2551 (12 ch.)
2	TDC LRS 2228A (8 ch. each)
8	ADC LRS 2249 (8 ch. each)
FASTBUS	
1	FASTBUS crate, power supply, fan, cables
1	LeCroy 1821, 1821/DEC interface, ATC, GAC cards, cables
1	Display module
6	LeCroy 1885 ADCs
NIM TRIGGER ELECTRONICS for	
2	NIM bin plus power supply
6	Disc. LRS 623B (8 ch. each)
12	Linear fan out LRS 428f (4 ch. each)
5	OR LRS 429a
1	QUAD LRS 365AL
2	Coincidence LRS 622

Figure Captions

Fig. 1 Location of the experiment at the antiproton accumulator.

Fig. 2 Experimental setup for the T861 test at the antiproton accumulator: (a) Side view of the setup, and (b) calorimeter cell structure.

Fig. 3 Distribution of total energy measured in the calorimeter for background events recorded during the T861 test (open histogram) compared with predictions from Monte Carlo simulated $\bar{p} \rightarrow e^- + \pi^0$ decays (shaded histogram). Note that the low energy tail in the predicted antiproton decay distribution is associated with events that are not fully contained within the calorimeter acceptance.

Fig. 4 Calorimeter energy depositions for four typical events recorded during the T861 test that have a total calorimeter energy in excess of 7 GeV.

Fig. 5 Distributions of calorimeter quantities used to distinguish signal from background, shown for events with total calorimeter energy in excess of 7 GeV (open histogram) and for Monte Carlo simulated $\bar{p} \rightarrow e^- + \pi^0$ decays (shaded histogram). The distributions (see text) are (a) the x - centroid [$\bar{x}$], (b) the y - centroid [$\bar{y}$], and (c) cluster multiplicity [N_{CLUST}].

Fig. 6 Examples of T861 events surviving the cuts $E_{TOT} > 7$ GeV, $\bar{x} < 4$ cm, $\bar{y} < 4$ cm, and $2 \leq N_{CLUST} \leq 3$.

Fig. 7 Proposed layout for the stage I antiproton decay search experiment showing (a) the overall layout of the experiment, and (b) the layout of the tracking and dE/dx detector components.

Fig. 8 Conceptual drawing of the vacuum chamber.

Fig. 9 Reconstructed π^0 peak in the E760 forward calorimeter.

Fig. 10 Schematic of the geometry of a scintillating fiber tracking plane.

Fig. 11 Schematic of the dE/dx counter arrangement.

Fig. 12 Pulse height distribution measured in four dE/dx scintillation planes used in the E715 experiment. These counters are of similar design to the dE/dx counters we are proposing. Single, double, and triple minimum ionizing peaks are clearly visible.

Fig. 13 Proposed calorimeter cell grouping for the trigger summers that can be used to implement a transverse momentum balance trigger.

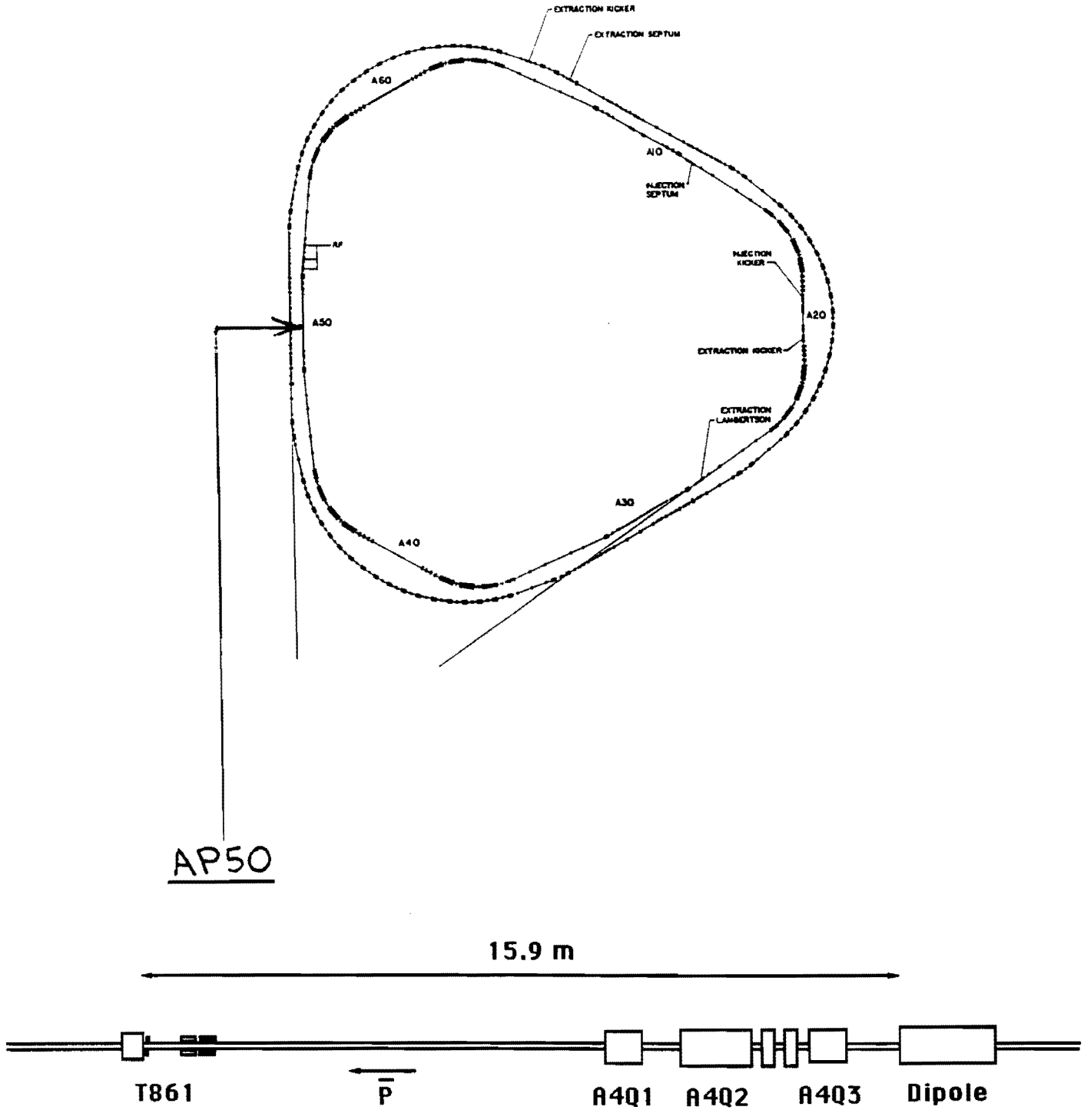
EXTRACTION KICKER
EXTRACTION SEPTUM
A60
A10
INJECTION SEPTUM
RF
INJECTION KICKER
A50
A20
EXTRACTION KICKER
EXTRACTION LAMBERTSON
A30
A40
AP50
15.9 m
T861
P
A4Q1
A4Q2
A4Q3
Dipole

Figure 1

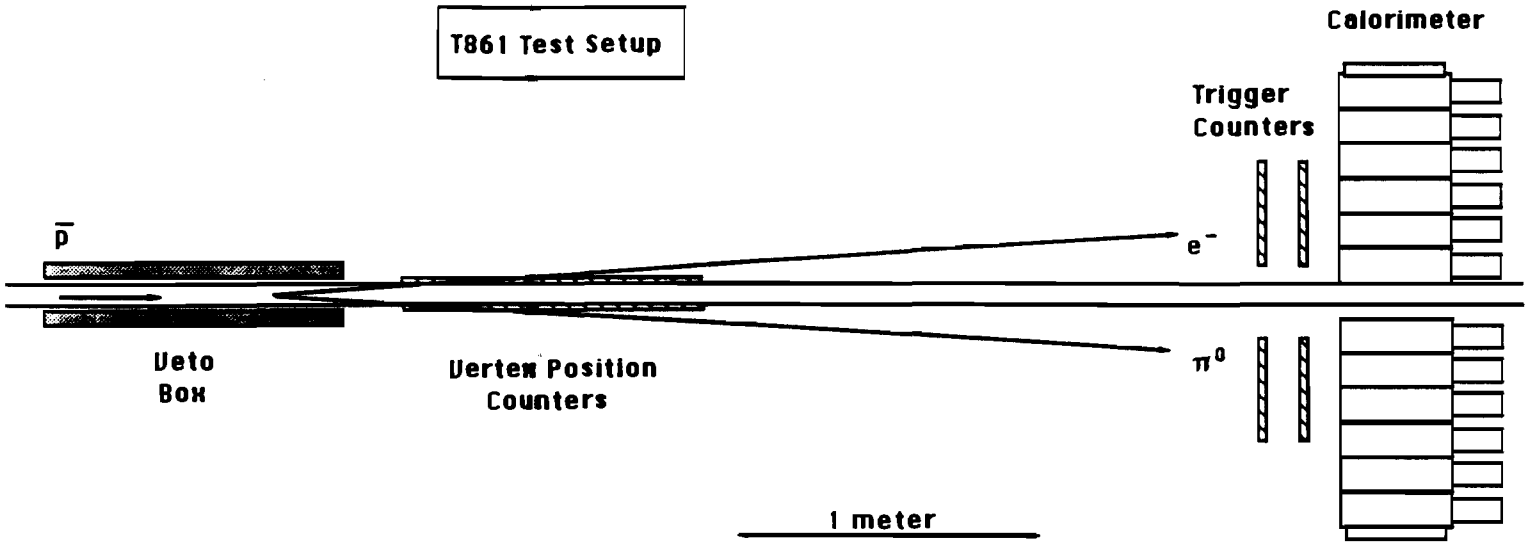
T861 Test Setup
Calorimeter
Trigger
Counters
$\bar{p}$
e^-
π^0
Veto
Box
Vertex Position
Counters
1 meter

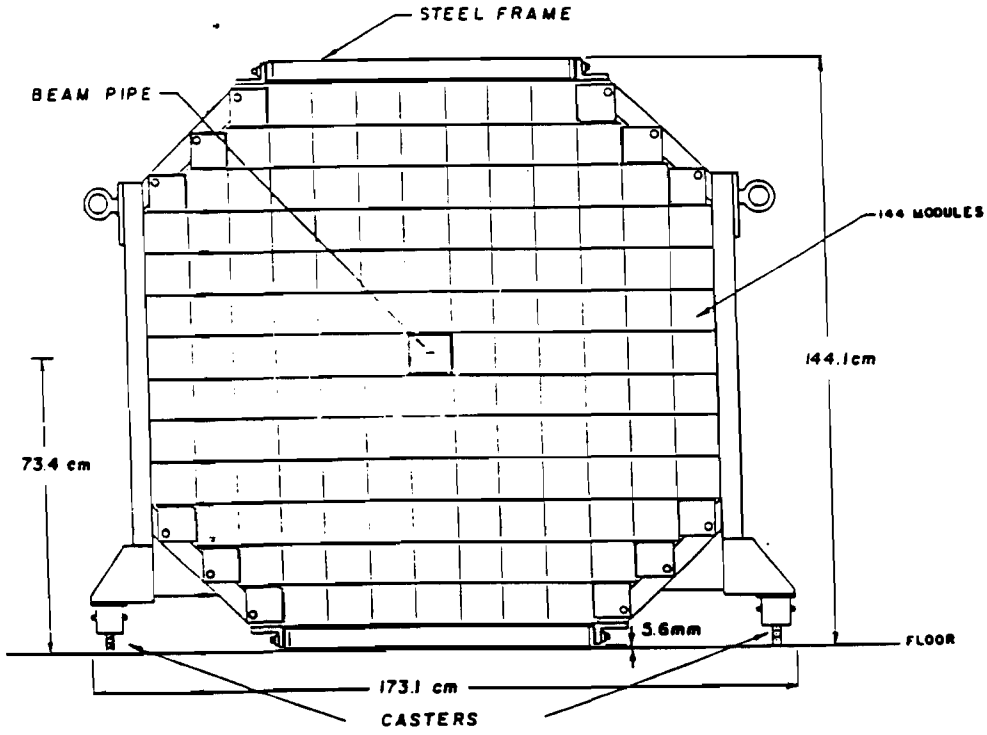
STEEL FRAME
BEAM PIPE
144 MODULES
144.1cm
73.4 cm
5.6mm
FLOOR
173.1 cm
CASTERS

Figure 2

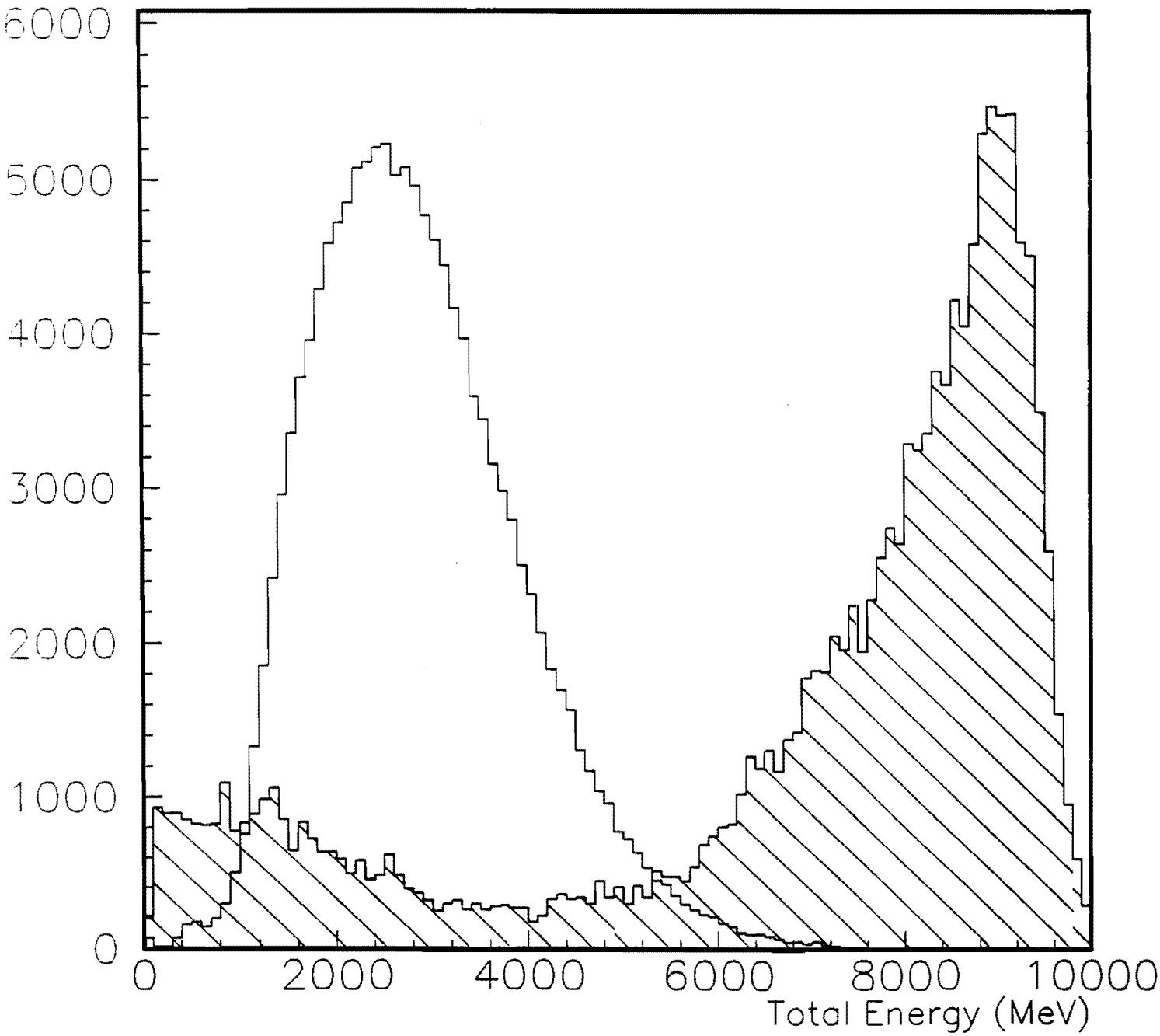
6000
5000
4000
3000
2000
1000
0
0
2000
4000
6000
8000
10000
Total Energy (MeV)

Figure 3

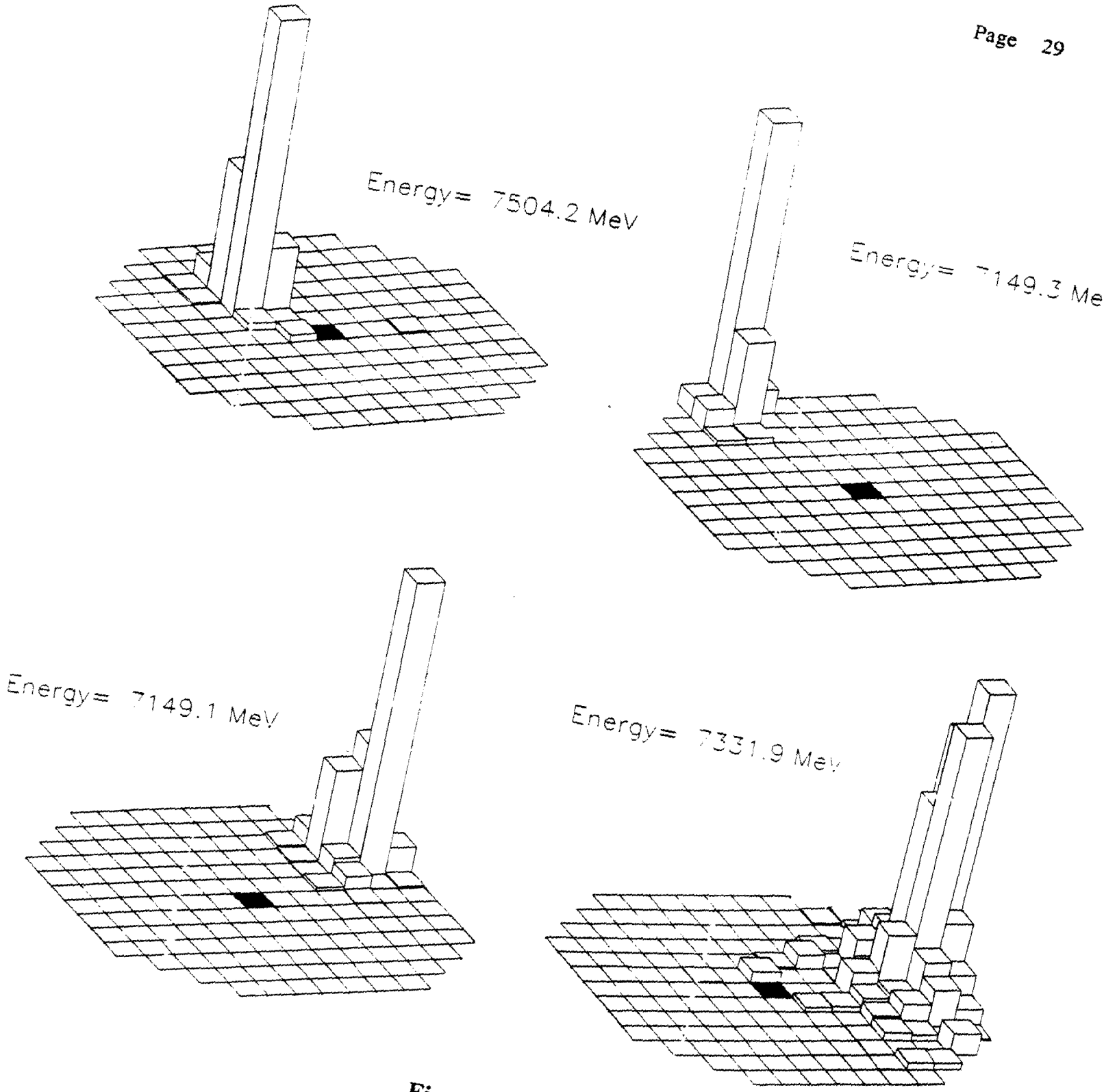
Energy= 7504.2 MeV
Energy= 7149.3 Me
Energy= 7149.1 MeV
Energy= 7331.9 MeV

Figure 4

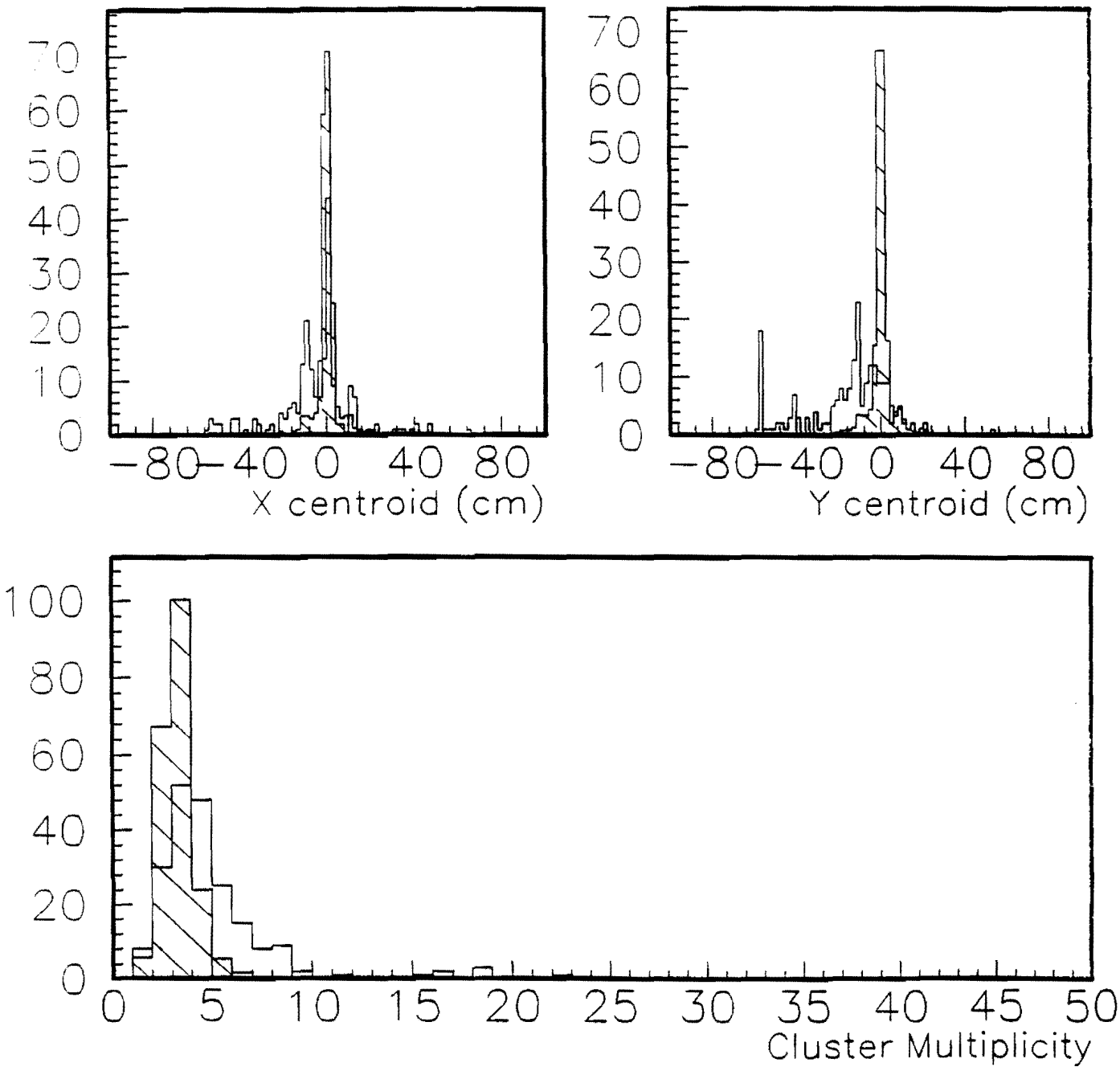
70
60
50
40
30
20
10
0
−80 −40 0 40 80
X centroid (cm)
70
60
50
40
30
20
10
0
−80 −40 0 40 80
Y centroid (cm)
100
80
60
40
20
0
0 5 10 15 20 25 30 35 40 45 50
Cluster Multiplicity

Figure 5

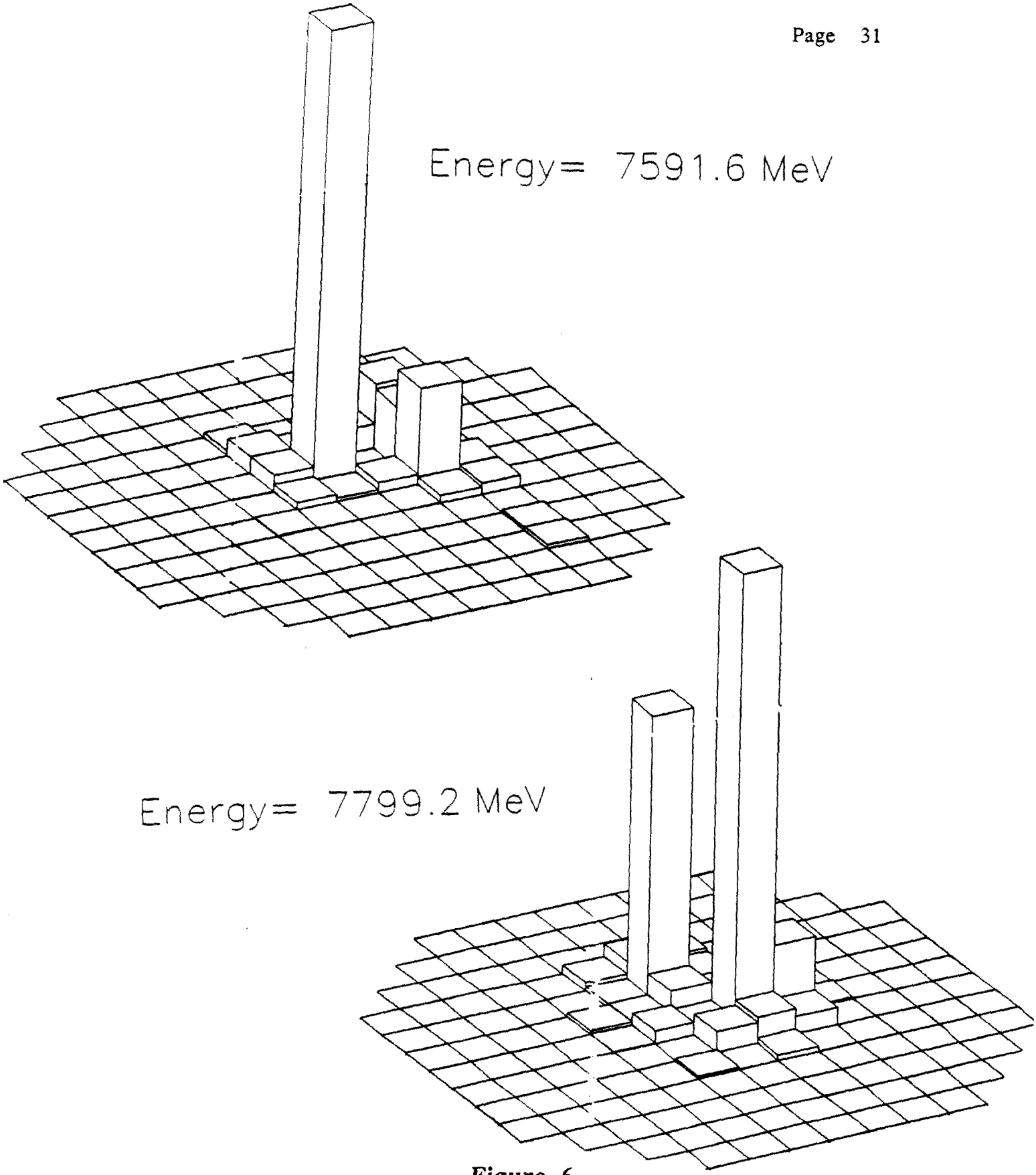

Figure 6

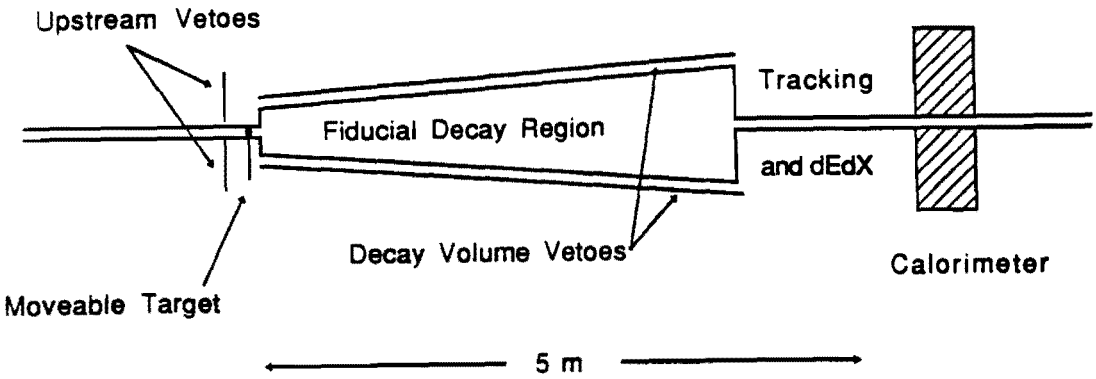
Upstream Vetoes
Fiducial Decay Region
Tracking
and dEdX
Decay Volume Vetoes
Calorimeter
Moveable Target
5 m

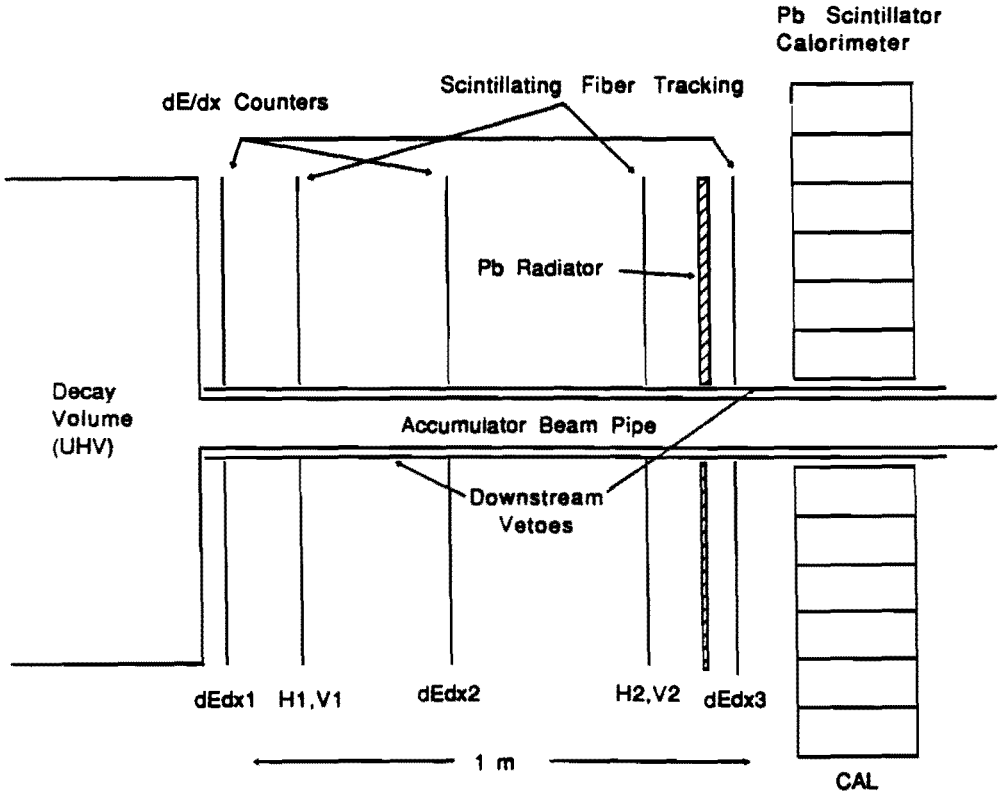
Pb Scintillator
Calorimeter
dE/dx Counters
Scintillating Fiber Tracking
Pb Radiator
Decay
Volume
(UHV)
Accumulator Beam Pipe
Downstream
Vetoes
dEdx1
H1,V1
dEdx2
H2,V2
dEdx3
1 m
CAL

Figure 7

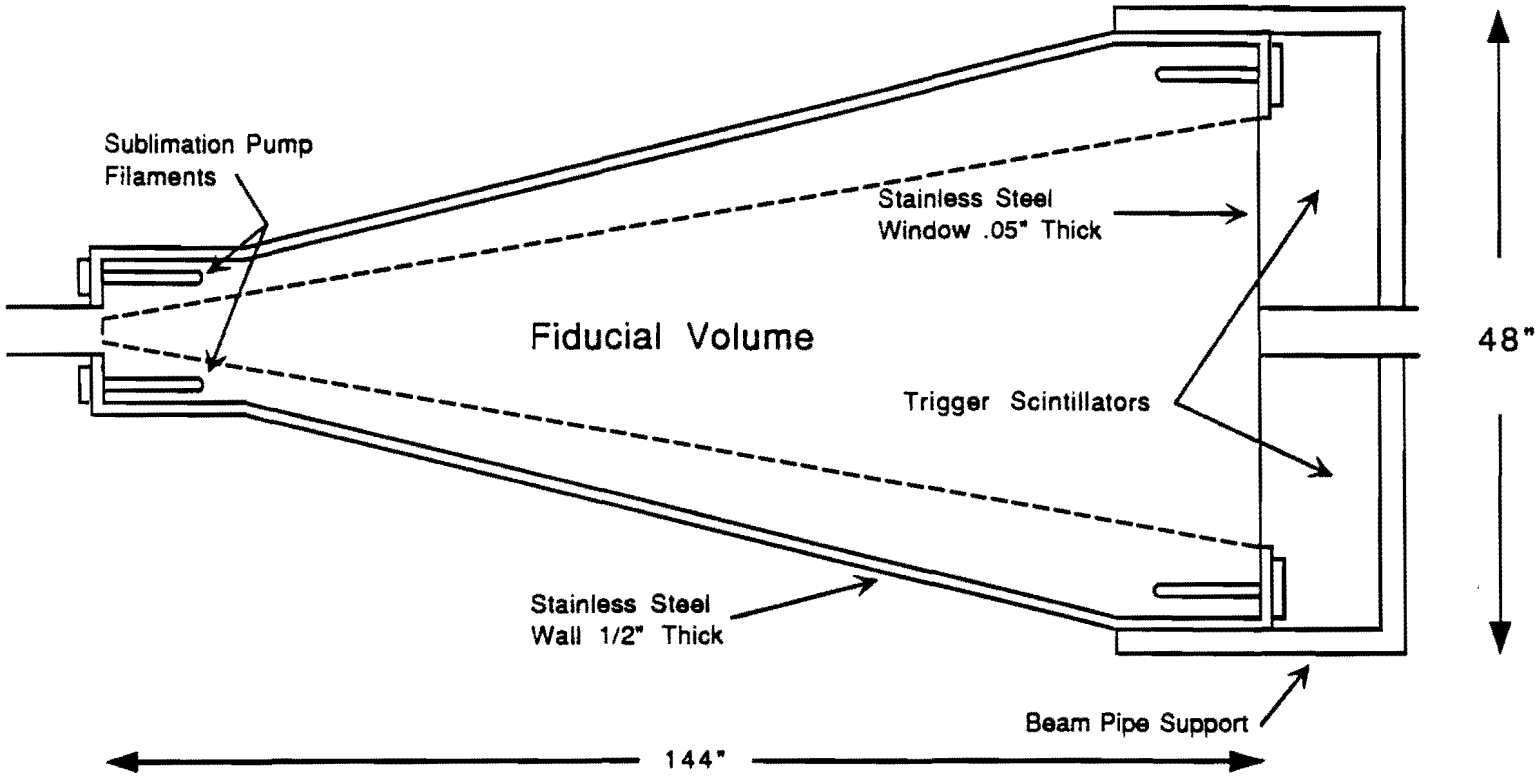

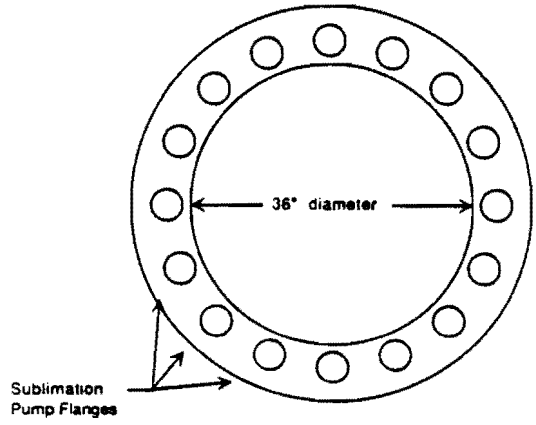

End Flange Detail

Figure 8

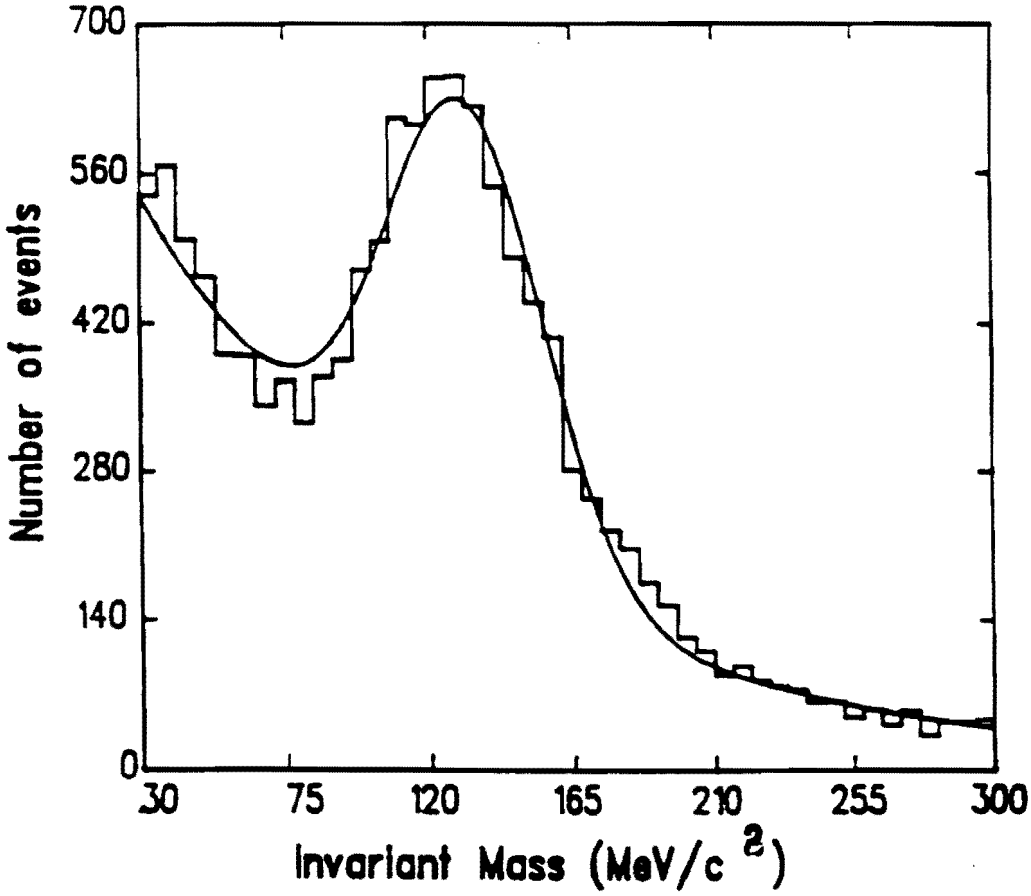
700
560
420
280
140
0
Number of events
30
75
120
165
210
255
300
Invariant Mass (MeV/c 2)

Figure 9

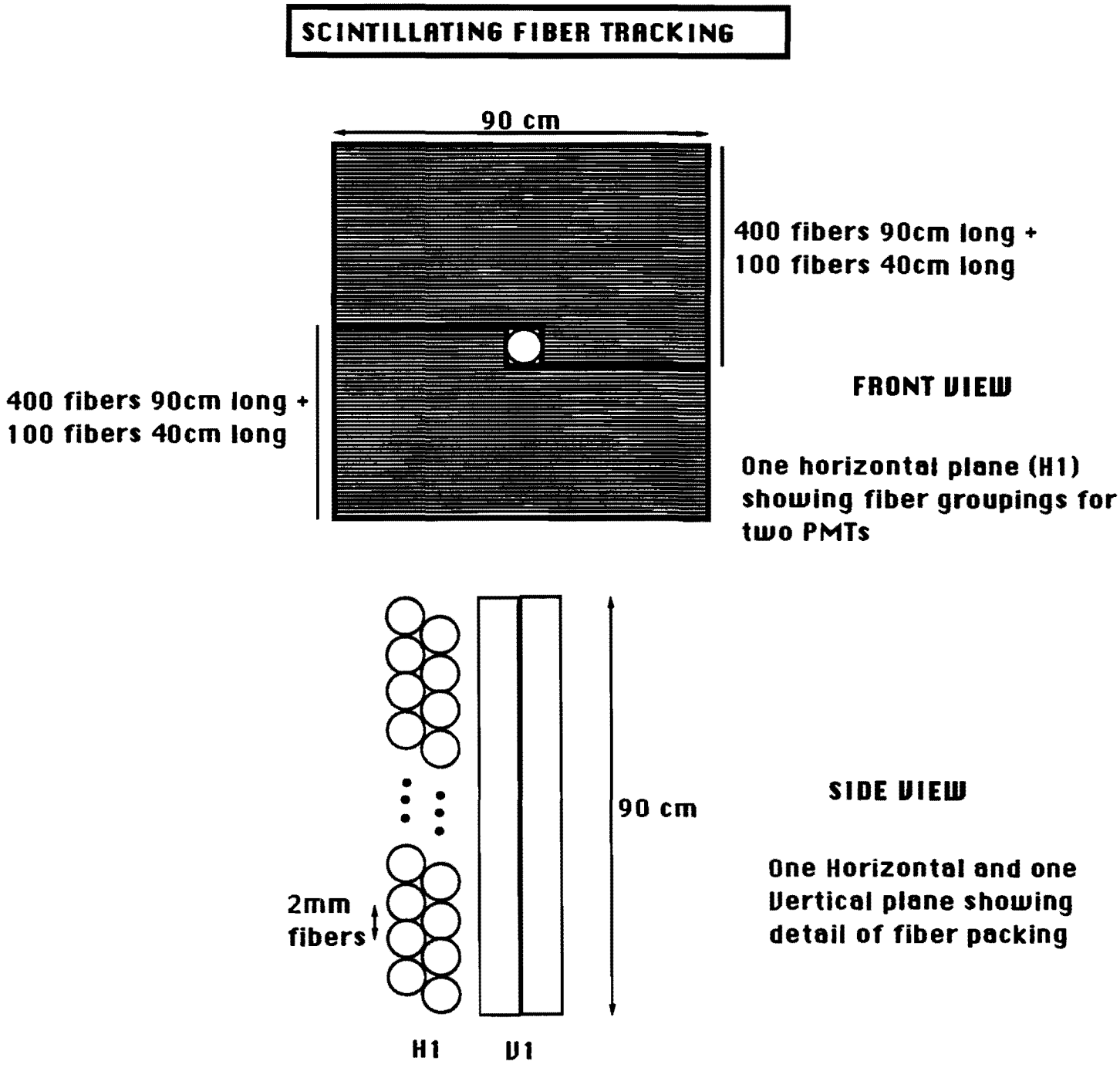
SCINTILLATING FIBER TRACKING
90 cm
400 fibers 90cm long +
100 fibers 40cm long
400 fibers 90cm long +
100 fibers 40cm long
FRONT VIEW
One horizontal plane (H1)
showing fiber groupings for
two PMTs
90 cm
2mm
fibers
SIDE VIEW
One Horizontal and one
Vertical plane showing
detail of fiber packing
H1
V1

Figure 10

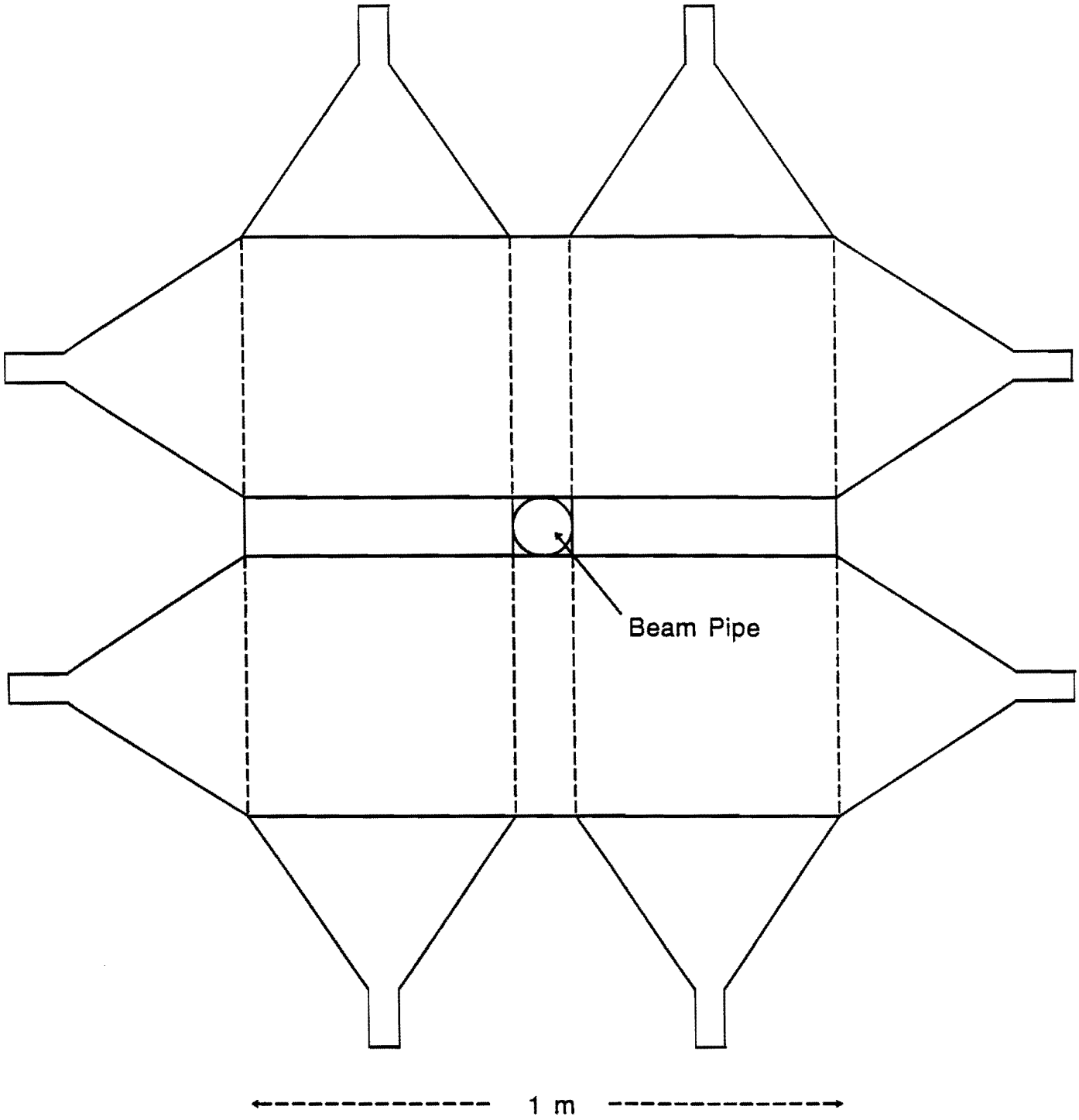

dEdx Counter Arrangement

Figure 11

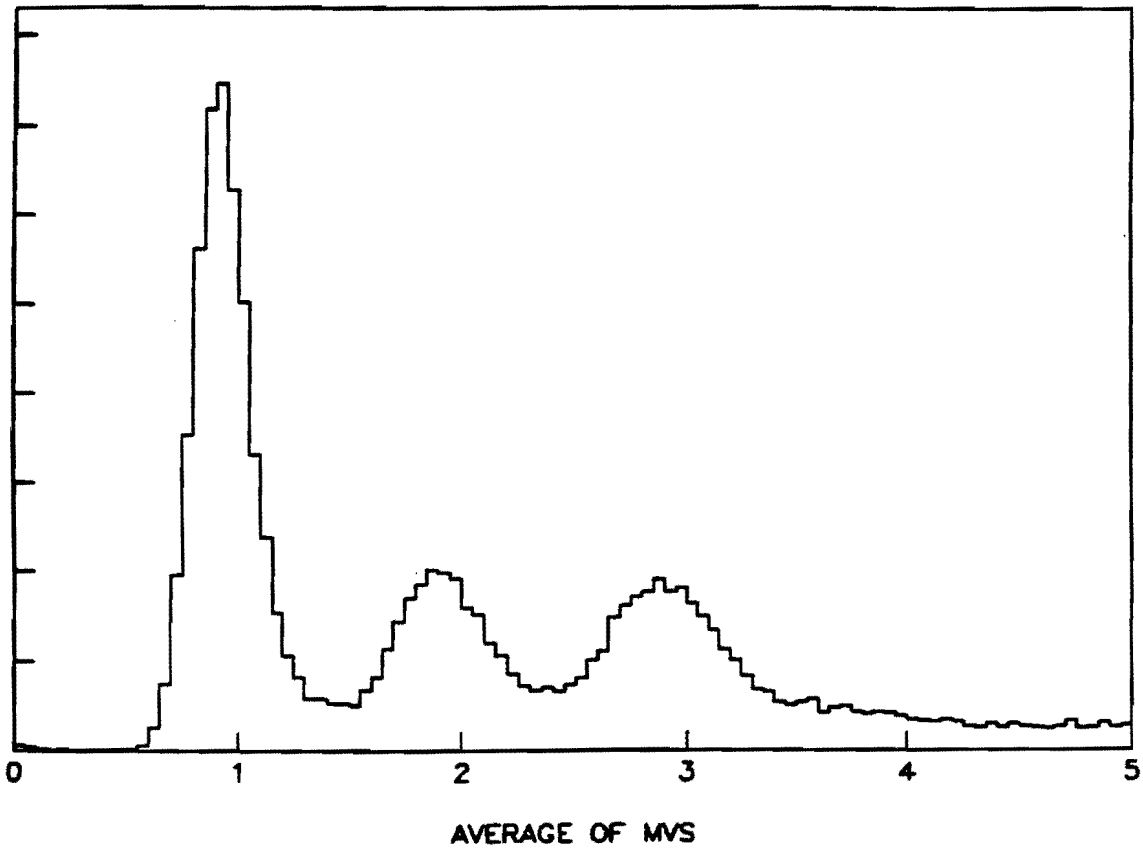

Figure 12

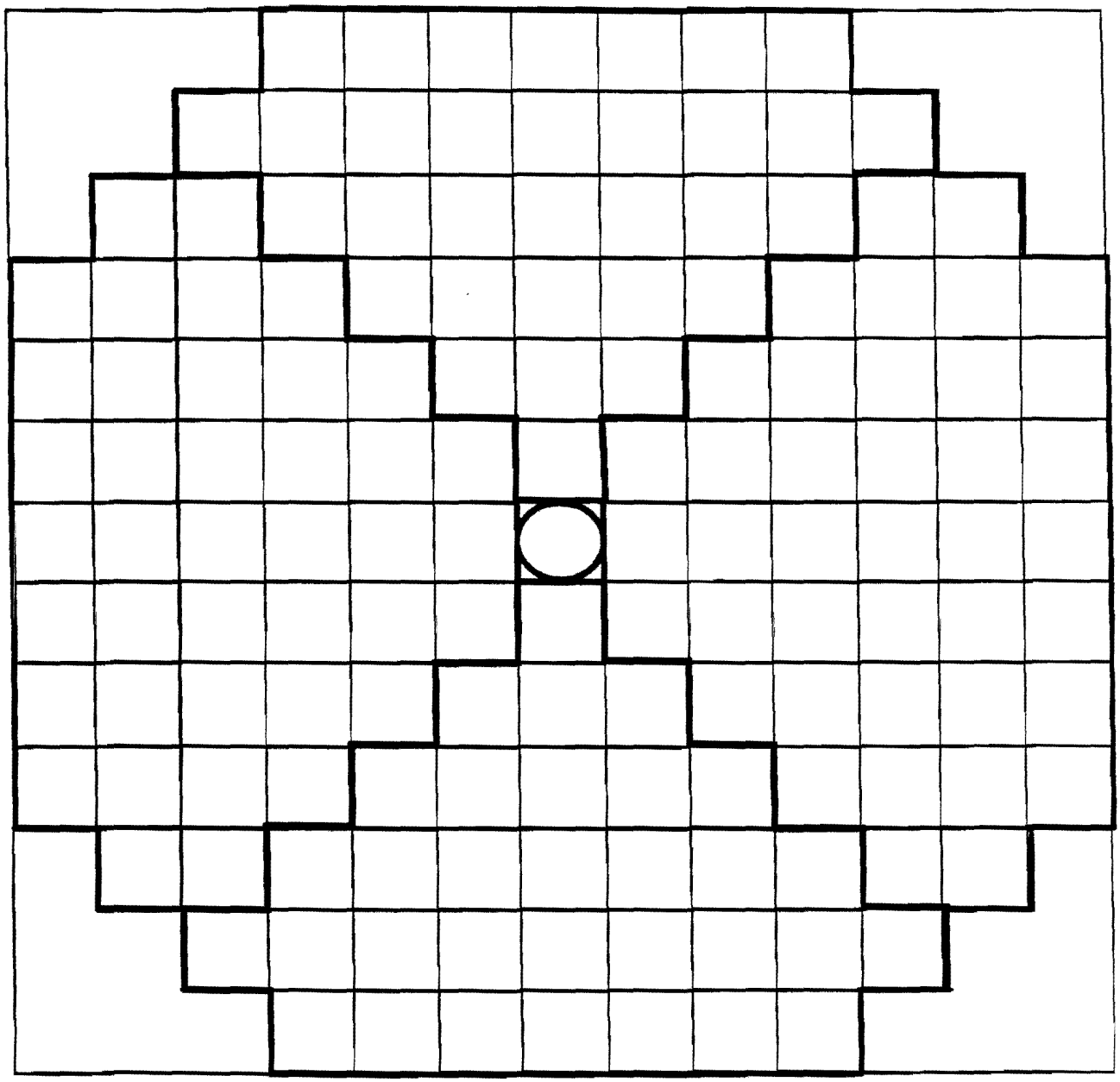

Figure 13